nature materials

ARTICLES

https://doi.org/10.1038/s41563-020-0728-2

A poly(thymine)–melamine duplex for the assembly of DNA nanomaterials

Qian Li[1,7], Jiemin Zhao[1,7], Longfei Liu[1,7], Sagun Jonchhe[2,7], Felix J. Rizzuto[3,7], Shankar Mandal[2], Huawei He[4], Sansen Wei[1], Hanadi F. Sleiman[3]✉, Hanbin Mao[2,5]✉ and Chengde Mao[1,6]✉

The diversity of DNA duplex structures is limited by a binary pair of hydrogen-bonded motifs. Here we show that poly(thymine) self-associates into antiparallel, right-handed duplexes in the presence of melamine, a small molecule that presents a triplicate set of the hydrogen-bonding face of adenine. X-ray crystallography shows that in the complex two poly(thymine) strands wrap around a helical column of melamine, which hydrogen bonds to thymine residues on two of its three faces. The mechanical strength of the thymine–melamine–thymine triplet surpasses that of adenine–thymine base pairs, which enables a sensitive detection of melamine at 3 pM. The poly(thymine)–melamine duplex is orthogonal to native DNA base pairing and can undergo strand displacement without the need for overhangs. Its incorporation into two-dimensional grids and hybrid DNA–small-molecule polymers highlights the poly(thymine)–melamine duplex as an additional tool for DNA nanotechnology.

The formation of a DNA duplex, a central molecule for all living systems, is predicted by the Watson–Crick base-pairing rules, G–C and A–T. Variation in the arrangement and orientation of hydrogen bonds leads to alternative DNA structures, which include triplexes[1], G-quadruplexes[2] and i-motifs[3,4]. Organic molecules or polymers can also interact with DNA[5,6] via the formation of hydrogen bonds with individual bases[7,8]. For example, the McLaughlin group designed a Janus-Wedge DNA triplex by using a polymer wherein each wedge residue formed a hydrogen-bonded triplet with a target base pair (bp)[9], whereas Bong and co-workers showed recognition between poly(thymine) (poly(T)) and a poly(melamine) peptide to generate a triplex[10]. Recently, Sleiman and co-workers found that cyanuric acid (CA) molecules could mediate the formation of a poly(A) triplex, in which three CA molecules bound to three adenines to generate a hexameric rosette[11]. Metal ions have also been shown to mediate DNA chain interactions[12,13]. For example, Hg^{2+} and Ag^{+} can bridge two T[14] or C[15] residues, respectively, to generate metal–DNA duplexes. Cu^{2+} can bridge between artificial oligonucleotides to generate biologically inspired ferromagnetic polymers[16]. These alternative structures present a rich chemistry for DNA and provide opportunities for materials applications and regulatory routes in biological processes.

Here we present experimental data to show that melamine (MA), an inexpensive small molecule, can mediate the association of two poly(T) strands to form antiparallel homoduplexes via T–MA–T hydrogen bonding. This interaction allows sensitive MA detection and can programme DNA tiles to assemble into designed nanostructures. These DNA–small-molecule assemblies are inherently more dynamic than Watson–Crick base pairs and enable tunable stabilities that demonstrate promising roles in developing stimuli-responsive DNA-based assemblies.

Structure of the poly(T)-MA duplex

MA contains three symmetrical edges that are hydrogen-bond complements to thymine. Thus, we hypothesized that MA may interact with poly(T) and assemble into duplexes[17,18] or triplexes[19,20] (Fig. 1). After annealing a mixture of poly(T) and MA, we performed native polyacrylamide gel electrophoresis (PAGE) (Fig. 2a–c). At 25 °C, poly(T) strands (T_{10}, T_{20} and T_{30}, which are 10, 20 and 30 bases long, respectively) migrate with expected mobilities in the absence of MA. However, in the presence of 10 mM MA, both T_{20} and T_{30} migrate more slowly, which suggests that T_{20} and T_{30} form multistranded complexes with MA. At elevated temperature (37 °C), the multistranded complexes dissociate and all poly(T) strands migrate as single strands. T_{10} retains the same electrophoretic mobility at 25 °C before and after MA addition, due to the low melting temperature of short strands with MA. This length and temperature dependence of mobility is mirrored by the native B-form of DNA.

To determine the number and relative orientation of DNA strands in poly(T)–MA complexes, we prepared a 52-base-long hairpin molecule, H (Fig. 2d,e). It contains a Watson–Crick hairpin domain in the middle and two T_{20} domains (black) at both ends. We hypothesized that H should form a three-stranded complex if poly(T)–MA was a triplex, and that H would remain monomeric (for antiparallel duplex) or form a two-stranded complex (for parallel duplex) if poly(T)–MA was a duplex. In PAGE, H showed as a sharp band and ran slightly faster in the presence of MA than it did in the absence of MA (Fig. 2d,e). This mobility difference indicated that strand H formed a compact monomer in the presence of MA, which suggests that the poly(T)–MA was an antiparallel duplex. Furthermore, when H was combined with T_{20} and 10 mM MA, PAGE analysis showed the presence of only H–MA and $(T_{20})_2$–MA, which suggests that antiparallel duplexes were formed exclusively in

[1]Department of Chemistry, Purdue University, West Lafayette, IN, USA. [2]Department of Chemistry and Biochemistry, Kent State University, Kent, OH, USA. [3]Department of Chemistry, McGill University, Montréal, Québec, Canada. [4]Biological Science Research Center, Southwest University, Chongqing, China. [5]Advanced Materials and Liquid Crystal Institute, Kent State University, Kent, OH, USA. [6]College of Pharmaceutical Sciences, Southwest University, Chongqing, China. [7]These authors contributed equally: Qian Li, Jiemin Zhao, Longfei Liu, Sagun Jonchhe, Felix J. Rizzuto. ✉e-mail: hanadi.sleiman@mcgill.ca; hmao@kent.edu; mao@purdue.edu

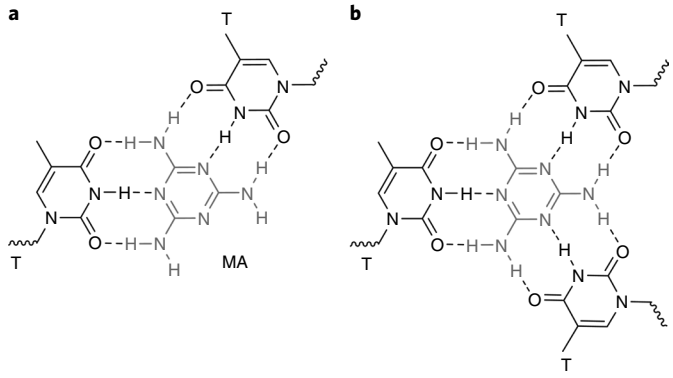

Fig. 1 | Potential hydrogen-bonding complexes between MA and T. a,**b**, A T_2–MA heterotriplet (**a**) and a T_3–MA heteroquadruplet (**b**) will lead to a poly(T) homoduplex and homotriplex, respectively. There are three hydrogen bonds between each T and MA. Experimental evidence supports the structure in **a**.

solution. We attribute the preferential formation of a duplex over a triplex to steric hindrance and strong electric repulsion among the DNA chains.

Circular dichroism (CD) spectra suggested that poly(T)–MA exhibited a chiral secondary structure (Supplementary Fig. 1). Although all poly(T)–MA complexes and poly(T) single strands displayed a positive Cotton effect centred at ~275 nm and a negative Cotton effect at ~250 nm, the poly(T)–MA complexes exhibited a higher peak and a shallower trough than those of single poly(T) strands. When compared with three major DNA duplex conformations (A, B and Z forms), poly(T)–MA and B-form DNA duplexes exhibit similar features, although their molar ellipticities are distinct: B-form DNA shows similar intensities for both positive (at 275 nm) and negative (at 245 nm) signals, whereas poly(T)–MA displays a high peak and a shallow trough, which suggests the formation of a distinct secondary structure for this poly(T)–MA duplex.

Dynamic light scattering (DLS) confirmed that no large particles were present in a solution of poly(T)–MA, which further indicates that the poly(T)–MA is a discrete duplex, as opposed to a polymer, in solution (Supplementary Fig. 2). To verify the 2:1 T:MA stoichiometry in the native (that is, not exclusive to the hairpin) structure, we varied the mole fraction of T_{50} to MA (where 1 equiv. corresponds to 50 molecules) and analysed the solutions by CD spectroscopy. A Job plot[21,22] indicated that the ratio of T_{50}:MA was 2:1 in solution (Supplementary Fig. 3), which reinforces that MA is complexed at only two of its three hydrogen-bonding faces.

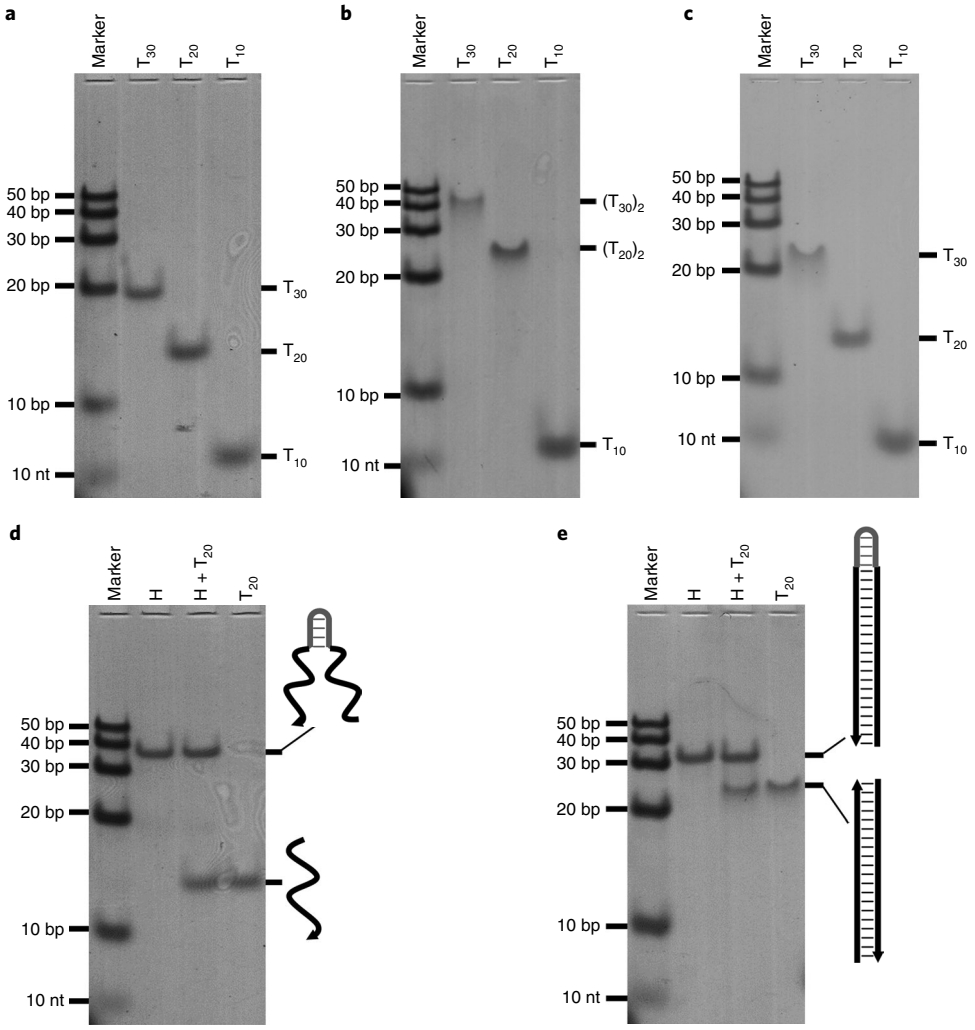

Fig. 2 | Analysis of the poly(T)–MA interaction by native PAGE. a–**c**, Varying the concentration of MA or the temperature: 0 mM MA at 25 °C (**a**), 10 mM MA at 25 °C (**b**), and 10 mM MA at 37 °C (**c**). **d**,**e**, Monitoring DNA folding of a DNA hairpin mediated by MA: 0 mM MA at 25 °C (**d**) and 10 mM MA at 25 °C (**e**). Sample compositions and the band identities are indicated above and beside the gel images, respectively. nt, nucleotide.

Interestingly, the third face of the complexed MA could be accessed by other hydrogen-bonding molecules. The addition of an equimolar portion of uric acid to T_{50}–MA generated a unique CD spectrum, with an induced CD signal from uric acid (Supplementary Fig. 4). No substantial increase in particle size was observed by DLS, which suggests that T_{50}–MA maintains its structure on uric acid binding to the third face of MA to generate a duplex that incorporates two small molecules.

X-ray crystallography unambiguously revealed the detailed structure of poly(T)–MA (Fig. 3). Single crystals were obtained from solutions that contained T_6 and MA at 20 °C by the hanging-drop vapour-diffusion method[23] (see Supplementary Fig. 6 for a crystal containing T5 and MA) and the structure of T_6–MA was resolved to a resolution of 2.42 Å by molecular replacement (Supplementary Table 2). Two T_6 strands complexed with six MA molecules to form a half-turn, right-handed, antiparallel duplex, which was composed of six consecutive T–MA–T triplets (Supplementary Fig. 7). MA interacted with two T residues by three hydrogen bonds to each T (O2, N3 and O4 of thymine), as shown in Fig. 3d. In each T–MA–T segment, all the atoms were approximately coplanar. The geometry and hydrogen-bond lengths within a single T–MA–T triplet resemble those of a C-G-C^+ triplet with T in the places of C and C^+ and MA in the place of G (Supplementary Fig. 8)[1].

Interestingly, the morphology of the T_6–MA duplex is similar to that of a DNA triplex, wherein the two T_6 strands resemble the orientation of two outer poly(T)/(C) strands and the central MA column resembles the poly(A)/(G) strand[1]. The morphology is thus distinct from the geometries of A- and B-form DNA duplexes (Supplementary Table 3)[24]. With an average twist of 30° for the T_6–MA duplex, one turn of an extended poly(T)–MA duplex has a length of 12 bp. In the crystal, the duplexes stack in a tail-to-head fashion, which results in uninterrupted, infinite columns of discrete duplexes across the crystal lattice (Fig. 3f,g). Duplexes in neighbour columns fit into the major grooves of each other (Fig. 3e). Such groove fitting leads to a relative 60° rotation between two interacting duplexes.

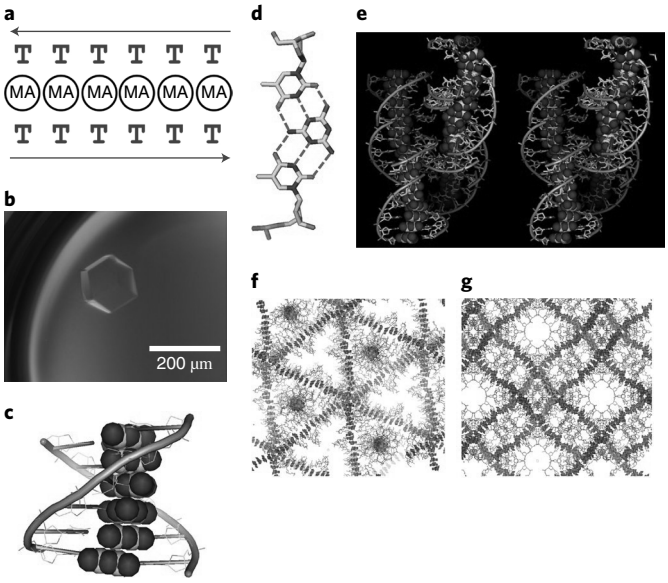

Fig. 3 | Crystallographic study of the T_6–MA complex. a, Schematic drawing of the T_6-MA duplex. Arrowheads indicate the 3′ ends of the DNA strands. **b**, An optical image of the T_6–MA crystal. **c**, Structural model of the T_6–MA duplex. Two DNA strands are shown with golden ribbon backbones and MA moieties are shown as blue/green spheres. **d**, Details of an MA-mediated T-T bp. Hydrogen bonds are represented by dashed lines. **e**, A stereo image showing that the poly(T)–MA duplexes fit within the major grooves of each other in the crystal. **f**,**g**, Crystal packing in the T_6–MA crystal viewed along the three- (**f**) and four-fold (**g**) screw axes, respectively; MAs are highlighted blue.

Tunable thermal stability and cooperativity

Both DNA length and MA concentration substantially and positively impacted the stability of poly(T)–MA duplexes. The formation of the poly(T)–MA duplex accompanied an absorbance decrease at ~260 nm (Supplementary Fig. 9). This hypochromic effect provided a convenient method to measure the stability of the poly(T)–MA complex (Supplementary Fig. 10). In the presence of 10 mM MA, the melting temperatures (T_m) were 21.5, 36.0 or 39.8 °C for T_{10}–MA, T_{20}–MA or T_{30}–MA, respectively (Supplementary Fig. 10a). For T_{30}–MA, T_m increased from 19.8 to 33.0 to 39.8 °C as the MA concentration was increased from 1 to 5 to 10 mM (Supplementary Fig. 10b). Without MA, no clear hypochromic transition was observed.

The solution pH was also observed to be a determinant in poly(T)–MA duplex stability (Supplementary Fig. 10c). When pH changed from 8.0 to 5.0, the T_m of the T_{30}–MA duplex increased from 39.8 to 53.3 °C, presumably due to the protonation of MA ($pK_a = 5.1$) (ref. [25]) under acidic conditions (Supplementary Fig. 11). Electrostatic attraction between the positive charge on the protonated MA and the electron-rich keto oxygens in the thymine bases or the negative charges of the DNA backbones might help to stabilize the poly(T)–MA duplex at lower pH values. Interestingly, Mg^{2+}, a divalent cation, only moderately enhanced the poly(T)–MA duplex stability (Supplementary Figs. 10d and 12).

The cooperative nature of native DNA folding was also observed in poly(T)–MA duplexes. With varying concentrations of MA, CD spectroscopy showed a short induction period in the association of MA with poly(T), followed by exponential growth (Supplementary Fig. 13). These curves suggest a cooperative assembly process[26], wherein elongation of the central MA column is preceded by a nucleation step, as opposed to a stepwise MA association[27,28]. This phenomenon scaled with the length of poly(T): longer strands exhibited a shorter induction period. Longer strands also produced a more-intense CD signal (for the same concentration of thymine bases), which suggests that the secondary structure propagates throughout the poly(T)–MA duplex. Consistent with a cooperative folding mechanism, melting curves also displayed hysteresis (Supplementary Fig. 10e).

Dynamic strand displacement

The poly(T)–MA duplex was less stable thermodynamically than poly(A)–poly(T) duplex, but more stable than a poly(A)–poly(T)–poly(T) triplex of the same length (Supplementary Fig. 14). For instance, when poly(A), poly(T) and MA were combined, poly(T) associated with poly(A) to form a conventional poly(A)–poly(T) duplex instead of a poly(T)–MA duplex. Likewise, when the poly(T)–MA duplex and poly(A) were mixed, poly(A) displaced the MA to generate a poly(A)–poly(T) duplex and release MA (Supplementary Fig. 14a). In no experiments was triplex DNA observed (Supplementary Fig. 15a). A thermal denaturation experiment confirmed that a conventional DNA duplex was more stable than poly(T)–MA (Supplementary Fig. 15b): the T_m of a A_{20}-T_{20} duplex was 52.5 °C, nearly 20 °C higher than the T_m of a T_{20}–MA duplex (36.0 °C).

MA forms a two-dimensional (2D) hydrogen-bonding network in the presence of CA[29]. We hypothesized that strand displacement akin to the addition of poly(A) would also occur on the addition of CA to poly(T)–MA, leading to the precipitation of CA–MA and regenerate free poly(T) in solution. Indeed, when CA (5 mM) was added to a solution of T_{15}–MA (5 mM MA), a white solid

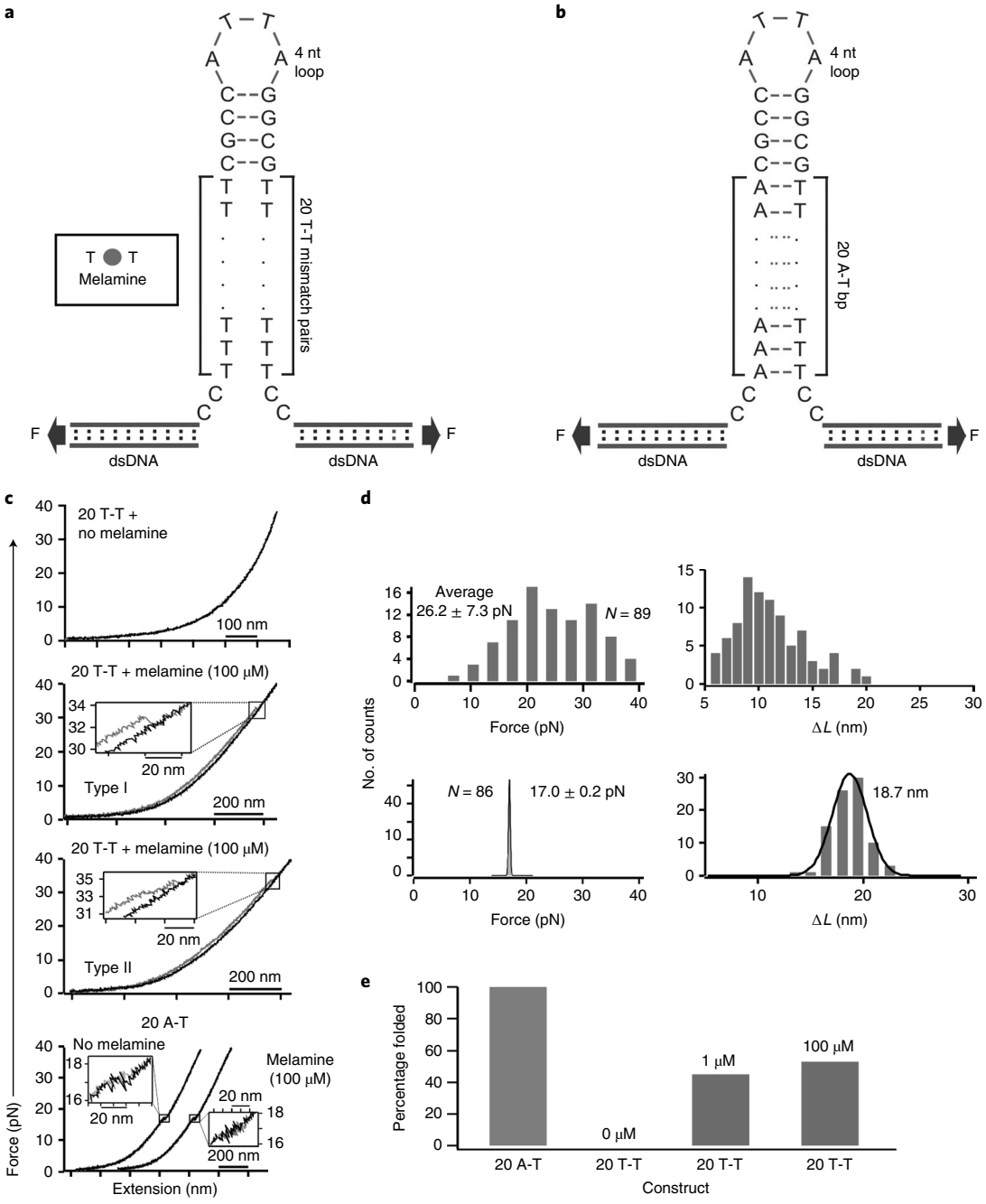

Fig. 4 | Mechanical properties of poly(T)–MA duplexes. a, Schematic of the DNA construct that contains 20 T-T mismatched pairs for the T–MA–T formation. **b**, Schematic of the control DNA construct that contains 20 A-T bp in the hairpin stem. **c**, Representative *F–X* curves of the 20 T-T and 20 A-T DNA constructs without and with MA (100 μM). Stretching and relaxing events are represented by coloured and black traces, respectively. In the bottom panel, the two sets of *F–X* curves are offset in the *x* axis for clarity. **d**, RF and the Δ*L* histograms of the 20 T-T construct in the presence of 100 μM MA (top) and those of the 20 A-T construct in the absence of MA (bottom). Solid curves depict Gaussian fittings. **e**, Percentage of folded species in different constructs without and with MA.

precipitated; however, no signal that corresponded to free T_{15} or T_{15}–MA was observed in the CD spectrum of the supernatant (Supplementary Fig. 16a). An infrared spectrum of this precipitate, compared with independently generated CA–MA, suggested that T_{15} was incorporated into the CA–MA matrix (Supplementary Fig. 16b). The addition of A_{15} to the solid that contained T_{15}–MA–CA led to a CD trace consistent with $T_{15}A_{15}$ in the supernatant. Poly(T) thus precipitates within the MA–CA matrix on the addition of CA to poly(T)–MA and can be re-extracted into solution with the addition of poly(A) (Supplementary Fig. 14b).

Mechanical properties

Mechanical properties of the poly(T)–MA duplex were examined by single-molecule mechanical unfolding experiments (Fig. 4)[30,31]. We synthesized a DNA construct that contained an unstable DNA hairpin consisting of a 4-bp G-C stem with a tetraloop (Fig. 4a). The G-C stem was extended by 20 T-T mismatch pairs (Supplementary Fig. 17), which would form a T_{20}–MA duplex in the presence of MA. The entire construct was sandwiched between two long double-stranded DNA (dsDNA) handles, which were anchored to two optically trapped beads via affinity linkages (Supplementary Fig. 17).

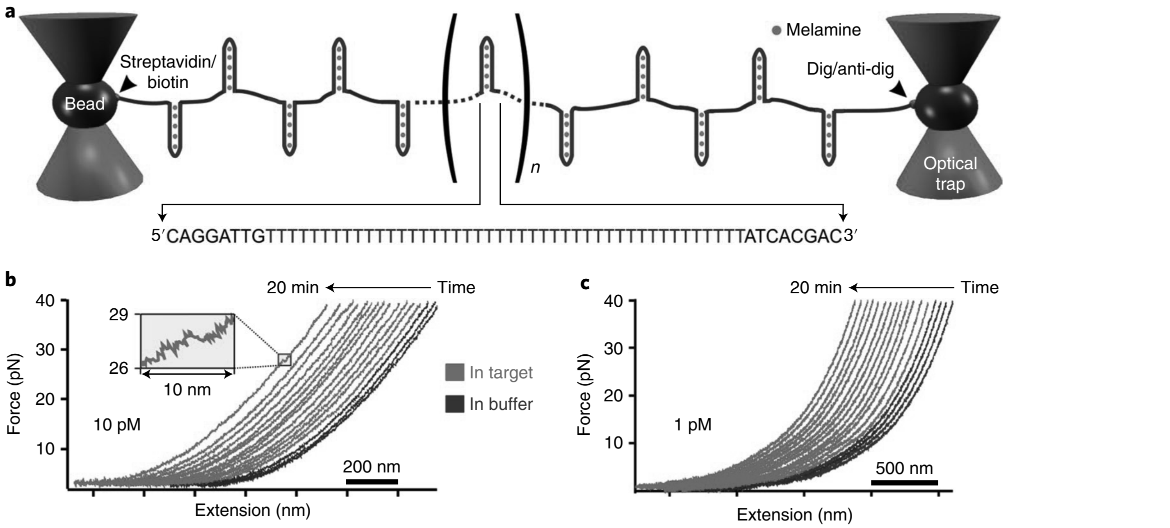

Fig. 5 | Mechanochemical sensing of MA using poly(T) templates. a, Schematic of the poly(T) sensing construct prepared by RCA. **b**,**c**, Unfolding *F–X* curves at 10 pM (**b**) and 1 pM (**c**) of the MA in 10 mM Tris and 100 mM KCl (pH 7.4) buffer. Blue and red traces indicate unfolding curves in the buffer and in the MA target, respectively. A time interval of 30 s was used between two *F–X* traces. **b**, Inset: unfolding of an MA binding event. See Supplementary Fig. 20 for the *F–X* traces of additional molecules. Dig/anti-dig, digoxigenin/anti-digoxigenin.

By moving one bead away from another with a loading speed of ~5.5 pN s^{-1} (10–30 pN range) in an Mg^{2+}-containing buffer, we increased the tensile force of the construct until structures were unfolded. We collected force–extension (*F–X*) curves for each single-molecule construct with an incubation time of 30 seconds between two successive *F–X* curves. The unfolding forces thus reflect mechanical stabilities of folded structures in the 20 T-T DNA construct with and without MA.

In the presence of 1 or 100 μM MA in the same buffer, the DNA construct revealed two types of unfolding features in the *F–X* curves. In the first type, the construct showed one unfolding feature, whereas in the second type, two sequential unfolding features were observed (Fig. 4c, middle two panels, and Supplementary Fig. 18). To confirm that these features were due to the unfolding of hairpins, we analysed the unfolding force (RF) and change in contour length (ΔL). The observed unfolding force (average 26.2 pN) (Fig. 4d, top left) was higher than that for A-T-rich DNA hairpins (17.0 pN) (ref. [30]), which suggests that the formation of poly(T)–MA complexes stabilizes the hairpin stem. Both RF and ΔL showed a wide distribution (RF, 8–38 pN; ΔL, 6–20 nm) (Fig. 4d, top panels). The species with a larger ΔL (~20 nm) were close to that expected for a fully folded hairpin (see Methods for the calculation), which suggests that most T-T mismatch pairs formed complexes with MA in this population. The species with smaller ΔL suggests that not all the T-T mismatch pairs formed complexes with MA, especially those at the base of the stem. This result is consistent with the reduced probability of hairpin formation at lower MA concentrations (Fig. 4e). In the absence of MA, no unfolding features were observed (Fig. 4c, top).

To directly compare the mechanical stability of poly(T)-MA with A-T base pairs, we evaluated the mechanical properties of a control DNA construct in which the 4-bp G-C stem was extended to include 20 A-T base pairs (Fig. 4b and Supplementary Fig. 17b). In the absence of MA, the *F–X* curves showed single unfolding features (Fig. 4c, bottom panel) at ~17 pN, in good agreement with reported values[30], whereas ΔL (18.7 nm) was close to that expected (Methods). In the presence of 100 μM MA, *F–X* curves identical to those without MA were observed (Fig. 4c, bottom panel, and Supplementary Fig. 19). These control experiments indicated that MA did not bind to A-T pairs and poly(T)–MA complexes were mechanically more stable than the A-T pairs with identical length. Mechanical anisotropy[32], which imparts structures with different mechanical stabilities as a function of the direction of applied force, explains the disparity between the measured mechanical and thermodynamic stabilities (Supplementary Fig. 15). During unfolding of the T–MA–T pairs, external force is perpendicular to the long axis of the stem. The increased unfolding force probably reflects the need to unzip extra π–π interactions between neighbouring T–MA–T pairs. In the X-ray structure (Fig. 3), the T–MA–T pairs, indeed, showed elongated π–π stacking along the long axis.

The mechanical unfolding of the T–MA–T pairs can be used in the single-molecule mechanochemical sensing[33] of MA molecules. The MA binding efficiency was low at low MA concentrations (Fig. 4e). We rationalized that more T residues in a sensing DNA would increase the chance for the MA to bind to T-T mismatch pairs and improve the limit of detection. We used rolling circle amplification (RCA)[34,35] to prepare a DNA construct that contained multiple T_{44} segments (Fig. 5a). It was labelled with biotin and digoxigenin at its two ends for attachment to two optically trapped particles (Fig. 5a). Binding of the MA to any of the T-T mismatch pairs in the sensing DNA would produce unfolding features similar to those observed in Fig. 4c. Indeed, at 10 pM MA, 100% sensing DNA showed MA binding within 20 minutes (Fig. 5b). At lower concentrations (for example 1 pM MA), less DNA (33%) bound to MA in the same time period (Fig. 5c and Supplementary Fig. 20). The limit of detection was estimated to be 3 pM (50% sensing DNA that shows analyte binding[36]) for the MA detection within 20 minutes. This value represents 1,000-fold improvement compared with previously reported MA sensing[37–39].

Nanostructure assembly

To explore the possible regulation effect of this poly(T)–MA DNA duplex on the self-assembly of DNA nanostructures[40], we investigated the 1D assembly of a double-crossover (DX) motif (Fig. 6a–c)[41]. Each side of the DX motif contained a blunt end and a single-stranded T_{10} (ssT_{10}) overhang. In the absence of MA, DX association was observed in neither PAGE (Supplementary Figs. 21 and 22)

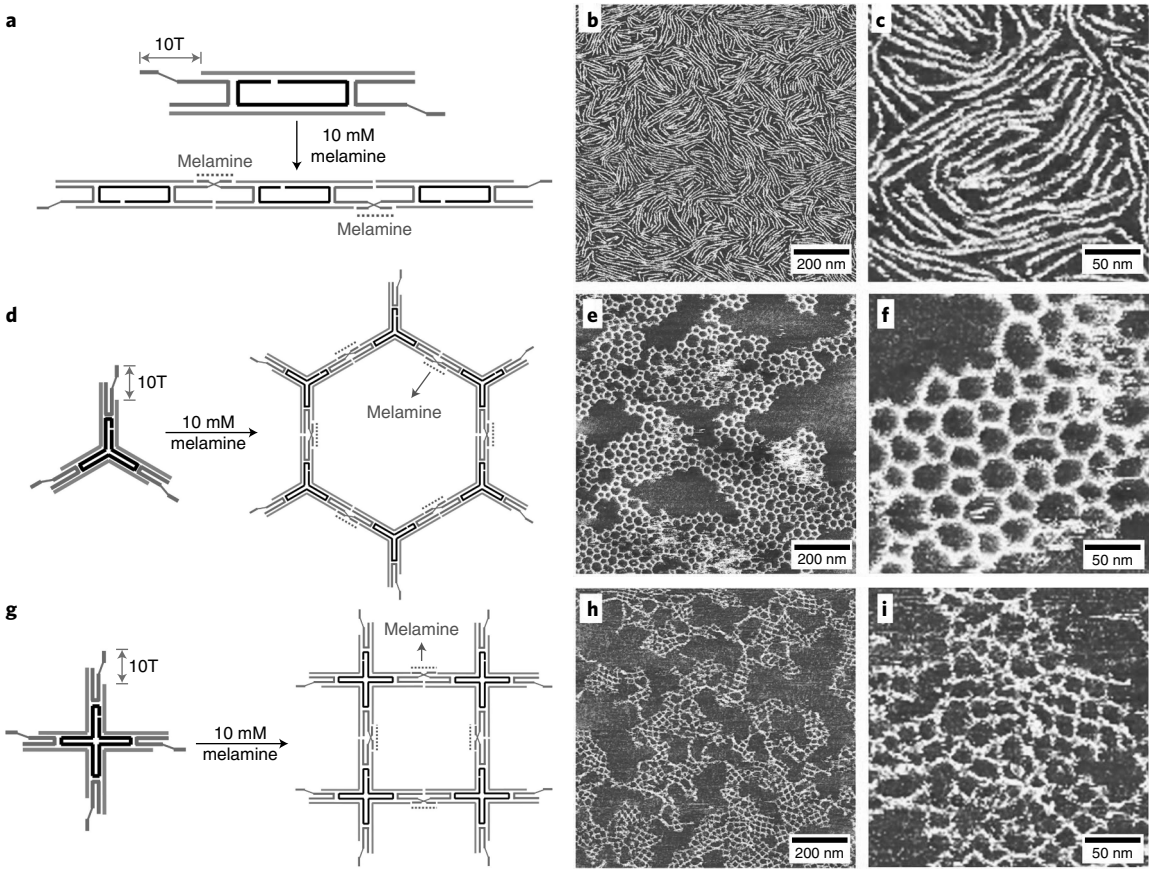

Fig. 6 | Applying poly(T)–MA to programme the self-assembly of DNA nanostructures. a–**c**, DNA DX assembles into 1D chains. **d**–**f**, DNA 3PS tiles assemble into hexagonal 2D arrays. **g**–**i**, DNA 4PS tiles assemble into tetragonal 2D arrays. **a**,**d**,**g**, Schemes of MA-mediated DNA self-assembly. Solid lines and dashed lines represent DNA strands and MA associated with poly-T strands, respectively. **b**,**c**,**e**,**f**,**h**,**i**, Pairs of AFM images at lower (**b**,**e**,**h**) and higher (**c**,**f**,**i**) magnifications of the 1D chains (**a**), hexagonal 2D arrays (**d**) and tetragonal 2D arrays (**g**), respectively.

nor atomic force microscopy (AFM) imaging (Supplementary Fig. 23a,b). On the addition of 10 mM MA, association of ssT_{10} overhangs assembled the DX tiles into 1D arrays, which were visualized by AFM imaging (Fig. 6b,c, and Supplementary Fig. 23c,d). To confirm the function of ssT_{10} overhang association, we prepared a control DX molecule (DX*) that was isomorphous to the aforementioned DX tile without ssT_{10} overhangs. DX* did not assemble into 1D arrays in the absence or presence of MA; instead, short DNA structures were observed in AFM imaging due to blunt-end stacking (Supplementary Fig. 24)[42,43].

We extended this strategy to regulate the formation of 2D DNA arrays from 3- and 4-point-star motifs (3PS (Fig. 6d–f) and 4PS (Fig. 6g–i), respectively)[44,45]. As with the DX motif, the outside end of each branch of the star motifs contained a blunt end and an ssT_{10} overhang (Fig. 6d,g). In the absence of MA, both motifs remained as individual motifs (Supplementary Figs. 22, 25 and 26). On the addition of 10 mM MA, both motifs assembled into 2D arrays (Fig. 6e,f,h,i). Although most DNA constructs exhibit specific thermal stabilities, the stabilities of structures that incorporate T–MA–T motifs can be altered by varying the MA concentration and poly(T) length.

Outlook

We have shown that MA can guide poly(T) to form an antiparallel, poly(T)–MA duplex in water. This structure has strong mechanical and tunable thermal stabilities during the unzipping of stacked T–MA–T pairs, which allow it to regulate the self-assembly of DNA nanostructures. Although poly(T) has previously been observed to interact with positively charged poly(melamine), this assembly relies on multivalency and electrostatic attraction[10]. In the present study, individual MA molecules are involved instead, and added entropic barriers are overcome to generate the poly(T)–MA duplex.

The ability to modulate the properties of DNA with a small molecule extends our knowledge of DNA chemistry beyond Watson–Crick base pairing and provides an alternative, inexpensive method to generate DNA-based architectures. It is conceivable that other small molecules with the correct hydrogen-bonding capability may interact with other bases in a similar fashion. Understanding how DNA interacts with other organic molecules may provide opportunities for applications in programmed supramolecular chemistry[46] and biosensing[47], to name a few, and may provide hints as to why DNA evolved into the universal, genetic materials for life[48].

Online content

Any methods, additional references, Nature Research reporting summaries, source data, extended data, supplementary information, acknowledgements, peer review information; details of author contributions and competing interests; and statements of data and code availability are available at https://doi.org/10.1038/s41563-020-0728-2.

Received: 29 May 2019; Accepted: 9 June 2020;
Published online: 13 July 2020

References

1. Frank-Kamenetskii, M. D. & Mirkin, S. M. Triplex DNA structures. *Annu. Rev. Biochem.* **64**, 65–95 (1995).
2. Rhodes, D. & Lipps, H. J. G-quadruplexes and their regulatory roles in biology. *Nucleic Acids Res.* **43**, 8627–8637 (2015).
3. Abou Assi, H., Garavís, M., González, C. & Damha, M. J. i-motif DNA: structural features and significance to cell biology. *Nucleic Acids Res.* **46**, 8038–8056 (2018).
4. Debnath, M., Fatma, K. & Dash, J. Chemical regulation of DNA i-motifs for nanobiotechnology and therapeutics. *Angew. Chem. Int. Ed.* **58**, 2942–2957 (2019).
5. Kang, S., Ohshima, K., Shimizu, M., Amirhaeri, S. & Wells, R. D. Pausing of DNA synthesis in vitro at specific loci in CTG and CGG triplet repeats from human hereditary disease genes. *J. Biol. Chem.* **270**, 27014–27021 (1995).
6. Dong, Y., Yang, Z. & Liu, D. Using small molecules to prepare vesicles with designable shapes and sizes via frame-guided assembly strategy. *Small* **11**, 3768–3771 (2015).
7. Davies, R. J. H. & Davidson, N. Base pairing equilibria between polynucleotides and complementary monomers. *Biopolymers* **10**, 1455–1479 (1971).
8. Li, C., Cafferty, B. J., Karunakaran, S. C., Schuster, G. B. & Hud, N. V. Formation of supramolecular assemblies and liquid crystals by purine nucleobases and cyanuric acid in water: implications for the possible origins of RNA. *Phys. Chem. Chem. Phys.* **18**, 20091–20096 (2016).
9. Chen, D., Meena, Sharma, S. K. & McLaughlin, L. W. Formation and stability of a Janus-wedge type of DNA triplex. *J. Am. Chem. Soc.* **126**, 70–71 (2004).
10. Zeng, Y., Pratumyot, Y., Piao, X. & Bong, D. Discrete assembly of synthetic peptide–DNA triplex structures from polyvalent melamine–thymine bifacial recognition. *J. Am. Chem. Soc.* **134**, 832–835 (2012).
11. Avakyan, N. et al. Reprogramming the assembly of unmodified DNA with a small molecule. *Nat. Chem.* **8**, 368–376 (2016).
12. Zhou, W., Saran, R. & Liu, J. Metal sensing by DNA. *Chem. Rev.* **117**, 8272–8325 (2017).
13. Gothelf, K. V., Thomsen, A., Nielsen, M., Cló, E. & Brown, R. S. Modular DNA-programmed assembly of linear and branched conjugated nanostructures. *J. Am. Chem. Soc.* **126**, 1044–1046 (2004).
14. Yamane, T. & Davidson, N. On the complexing of desoxyribonucleic acid (DNA) by mercuric ion. *J. Am. Chem. Soc.* **83**, 2599–2607 (1961).
15. Ono, A. et al. Specific interactions between silver(i) ions and cytosine–cytosine pairs in DNA duplexes. *Chem. Commun.* **2008**, 4825–4827 (2008).
16. Tanaka, K., Tengeiji, A., Kato, T., Toyama, N. & Shionoya, M. A discrete self-assembled metal array in artificial DNA. *Science* **299**, 1212–1213 (2003).
17. Mao, J., DeSantis, C. & Bong, D. Small molecule recognition triggers secondary and tertiary interactions in DNA folding and hammerhead ribozyme catalysis. *J. Am. Chem. Soc.* **139**, 9815–9818 (2017).
18. Vollhardt, D., Liu, F., Rudert, R. & He, W. Interfacial molecular recognition of dissolved thymine by medium chain dialkyl melamine-type monolayers. *J. Phys. Chem. B* **109**, 10849–10857 (2005).
19. Lange, R. F. M. et al. Crystal engineering of melamine–Imide complexes; tuning the stoichiometry by steric hindrance of the imide carbonyl groups. *Angew. Chem. Int. Ed.* **36**, 969–971 (1997).
20. Du, J., Wang, Z., Peng, X. & Fan, J. In situ colorimetric recognition of melamine based on thymine derivative-functionalized gold nanoparticle. *Ind. Eng. Chem. Res.* **54**, 12011–12016 (2015).
21. Renny, J. S., Tomasevich, L. L., Tallmadge, E. H. & Collum, D. B. Method of continuous variations: applications of job plots to the study of molecular associations in organometallic chemistry. *Angew. Chem. Int. Ed.* **52**, 11998–12013 (2013).
22. Ulatowski, F., Dąbrowa, K., Bałakier, T. & Jurczak, J. Recognizing the limited applicability of job plots in studying host–guest interactions in supramolecular chemistry. *J. Org. Chem.* **81**, 1746–1756 (2016).
23. Mikol, V., Rodeau, J.-L. & Giegé, R. Experimental determination of water equilibration rates in the hanging drop method of protein crystallization. *Anal. Biochem.* **186**, 332–339 (1990).
24. Dickerson, R. E. DNA structure from A to Z. *Methods Enzymol.* **211**, 67–111 (1992).
25. Dixon, J. K., Woodberry, N. T. & Costa, G. W. The dissociation constants of melamine and certain of its compounds. *J. Am. Chem. Soc.* **69**, 599–603 (1947).
26. De Greef, T. F. A. et al. Supramolecular polymerization. *Chem. Rev.* **109**, 5687–5754 (2009).
27. Smulders, M. M. J. et al. How to distinguish isodesmic from cooperative supramolecular polymerisation. *Chem. Eur. J.* **16**, 362–367 (2010).
28. Zhao, D. & Moore, J. S. Nucleation–elongation: a mechanism for cooperative supramolecular polymerization. *Org. Biomol. Chem.* **1**, 3471–3491 (2003).
29. Seto, C. T. & Whitesides, G. M. Self-assembly based on the cyanuric acid–melamine lattice. *J. Am. Chem. Soc.* **112**, 6409–6411 (1990).
30. Woodside, M. T. et al. Nanomechanical measurements of the sequence-dependent folding landscapes of single nucleic acid hairpins. *Proc. Natl Acad. Sci. USA* **103**, 6190–6195 (2006).
31. Koirala, D. et al. A single-molecule platform for investigation of interactions between G-quadruplexes and small-molecule ligands. *Nat. Chem.* **3**, 782–787 (2011).
32. Jonchhe, S. et al. Binding of a telomestatin derivative changes mechanical anisotropy of human telomeric G-quadruplex. *Angew. Chem. Int. Ed. Engl.* **58**, 877–881 (2019).
33. Koirala, D., Yu, Z., Dhakal, S. & Mao, H. Detection of single nucleotide polymorphism using tension-dependent stochastic behavior of a single-molecule template. *J. Am. Chem. Soc.* **133**, 9988–9991 (2011).
34. Fire, A. & Xu, S. Q. Rolling replication of short DNA circles. *Proc. Natl Acad. Sci. USA* **92**, 4641–4645 (1995).
35. Liu, D., Daubendiek, S. L., Zillman, M. A., Ryan, K. & Kool, E. T. Rolling circle DNA synthesis: small circular oligonucleotides as efficient templates for DNA polymerases. *J. Am. Chem. Soc.* **118**, 1587–1594 (1996).
36. Mandal, S., Koirala, D., Selvam, S., Ghimire, C. & Mao, H. A molecular tuning fork in single-molecule mechanochemical sensing. *Angew. Chem. Int. Ed. Engl.* **54**, 7607–7611 (2015).
37. Huang, H. et al. Visual detection of melamine in milk samples based on label-free and labeled gold nanoparticles. *Talanta* **85**, 1013–1019 (2011).
38. Qi, W. J., Wu, D., Ling, J. & Huang, C. Z. Visual and light scattering spectrometric detections of melamine with polythymine-stabilized gold nanoparticles through specific triple hydrogen-bonding recognition. *Chem. Commun.* **46**, 4893–4895 (2010).
39. Li, H., Somerson, J., Xia, F. & Plaxco, K. W. Electrochemical DNA-based sensors for molecular quality control: continuous, real-time melamine detection in flowing whole milk. *Anal. Chem.* **90**, 10641–10645 (2018).
40. Seeman, N. C. & Sleiman, H. F. DNA nanotechnology. *Nat. Rev. Mater.* **3**, 17068 (2017).
41. Fu, T. J. & Seeman, N. C. DNA double-crossover molecules. *Biochemistry* **32**, 3211–3220 (1993).
42. Liu, L., Li, Y., Wang, Y., Zheng, J. & Mao, C. Regulating DNA self-assembly by DNA–surface interactions. *ChemBioChem* **18**, 2404–2407 (2017).
43. Avakyan, N., Conway, J. W. & Sleiman, H. F. Long-range ordering of blunt-ended DNA tiles on supported lipid bilayers. *J. Am. Chem. Soc.* **139**, 12027–12034 (2017).
44. He, Y., Chen, Y., Liu, H., Ribbe, A. E. & Mao, C. Self-assembly of hexagonal DNA two-dimensional (2D) arrays. *J. Am. Chem. Soc.* **127**, 12202–12203 (2005).
45. He, Y. et al. Sequence symmetry as a tool for designing DNA nanostructures. *Angew. Chem. Int. Ed.* **44**, 6694–6696 (2005).
46. Vantomme, G. & Meijer, E. W. The construction of supramolecular systems. *Science* **363**, 1396–1397 (2019).
47. Sassolas, A., Leca-Bouvier, B. D. & Blum, L. J. DNA biosensors and microarrays. *Chem. Rev.* **108**, 109–139 (2008).
48. Krishnamurthy, R. Experimentally investigating the origin of DNA/RNA on early Earth. *Nat. Commun.* **9**, 5175 (2018).

Methods

Materials. MA was purchased from Sigma-Aldrich. Streptavidin and anti-digoxigenin-coated polystyrene beads were purchased from Spherotech. DNA sequences were designed by the computer program SEQUIN and all the schemes of DNA nanomotifs were drawn with the computer software Tiamat. All the oligonucleotides were purchased from IDT and purified by 10–20% denaturing PAGE. Oligonucleotides from all the tiles are listed below with their designated ratio and concentration during in situ assembly.

DNA sequences (5′–3′). T_5: TTTTT
T_6: TTTTTT
T_{10}: TTTTTTTTTT
T_{15}: TTTTTTTTTTTTTTT
T_{20}: TTTTTTTTTTTTTTTTTTTT
T_{30}: TTTTTTTTTTTTTTTTTTTTTTTTTTTTTT
T_{50}: TTTTTTTTTTTTTTTTTTTTTTTTTTTTTTTTTTTTTTTTTTTTTTTTTT
$T_{20}C_{10}$: TTTTTTTTTTTTTTTTTTTTCCCCCCCCCC
H: TTTTTTTTTTTTTTTTTTTTCGCCATTAGGCGT-TTTTTTTTTTTTTTTTTTT (hairpin sequence is underlined)
L2: CCAGGCACCATCGTAGGCTTGCCAGGCACCATCGTAGGCTTG
L3: AGGCACCATCGTAGGTTTCTTGCCAGGCACCATCGTAGGTTTCTT-GCCAGGCACCATCGTAGGTTTCTTGCC
L4: AGGCACCATCGTAGGTTTTCTTGCCAGGCACCATCGTAGGTTTT-CTTGCCAGGCACCATCGTAGGTTTTCTTGCCAGGCACCATCGTAG GTTTTCTTGCC
M: TAGCAACCTGCCTGGCAAGCCTACGATGGACACGGTAATGAC
M′: ACTATGCAACCTGCCTGGCAAGCCTACGATGGACACGGTAACG
S: GTCATTACCGTGTGGTTGCTATTTTTTTTTT
S′: CGTTACCGTGTGGTTGCATAGT
Oligo1: CTAGTGCATTAGGAAGCAGCCCAGCTAACCTTTTTTTTTTTTT TTTTTTTCGCCATTAGGCGTTTTTTTTTTTTTTTTTTTTCCAA AGAGCAAGACGTAGCCCAGCGCG
Oligo 2: TTTTCTGGGCTGCTTCCTAATGCA
Oligo 3: GGCCCGCGCTGGGCTACGTCTTGCTTTTT
Oligo 4: CTAGTGCATTAGGAAGCAGCCCAGCTAACCAAAAAAAAAAAA
Oligo 5: AAAAAAAACGCCATTAGGCGTTTT
Oligo 6: TTTTTTTTTTTTTTTTCCAAAGAGCAAGACGTAGCCCAGCGCG.

Motifs. DX: L2 + M + S (1:2:2)
DX*: L2 + M′ + S′ (1:2:2)
3PS: L3 + M + S (1:3:3)
4PS: L4 + M + S (1:4:4).

TAE/Mg^{2+} buffer. The TAE/Mg^{2+} buffer consisted of 40 mM tris base, 20 mM acetic acid, 2 mM EDTA, and 12.5 mM magnesium acetate; pH was adjusted to 8.0. This was used in the PAGE, thermal denaturation, AFM and mechanical stability experiments.

TA/Mg^{2+} buffer. The TA/Mg^{2+} buffer consisted of 40 mM tris base, 7.6 mM magnesium chloride; pH was adjusted to 8.0 with acetic acid. This was used in the CD and DLS experiments and those shown in in Supplementary Fig. 3.

Assembly of poly(T)–MA complexes. The DNA strand (T_{10}, T_{20}, T_{30} or T_{50}) and MA were mixed in TAE/Mg^{2+} or TA/Mg^{2+} buffer and cooled from 50 °C to 4 °C over 2 h. DNA strand H was employed in TAE/Mg^{2+} buffer and heated to 95 °C for 3 min and cooled on ice for 10 min before being mixed with MA and cooled from 50 °C to 4 °C over 2 h.

Native PAGE. Native PAGE that contained 20% polyacrylamide (19:1 acrylamide:bisacrylamide) was run on a FB-VE10-1 electrophoresis unit (FisherBiotech) at 25 °C (90 V, constant voltage). Each lane contained 1 μg of DNA in 20 μl of solution. TAE/Mg^{2+} buffer was used both as the running buffer and the buffer in the gel. After electrophoresis, the gels were stained with Stains-All (Sigma) and scanned with an HP scanner (Scanjet 4070 Photosmart). The duplex size markers were homemade by hybridizing complementary strands together.

Assembly of poly(T)–MA complexes at different pH. Before the annealing process, 1.0 M HCl was added to the mixture and the solution pH was adjusted to a desired value. Samples were then annealed from 50 °C to 4 °C over 2 h.

Thermal denaturation. The DNA strand and MA were dissolved in TAE/Mg^{2+} buffer (150 μl) and annealed from 50 °C to 4 °C over 2 h. TAE/Mg^{2+} or TA/Mg^{2+} buffer (with MA) was used as a blank. The thermal denaturation was monitored by an Agilent Technologies CARY Series UV-Vis-NIR spectrophotometer and the temperature was increased at a rate of 1 °C min^{-1} from 25 to 60 °C and then decreased at 1 °C min^{-1} from 60 to 4 °C. In all the measurements, the concentration of the thymine nucleotide was kept at 60 μM.

CD. The DNA strand and MA were dissolved in TAE/Mg^{2+} buffer (500 μl) and annealed from 50 to 4 °C over 2 h. TAE/Mg^{2+} buffer (MA) was used as a blank. The CD spectra were measured on a Jasco J-1500 CD spectrometer at room temperature (230–350 nm range, 50 nm min^{-1} scan rate, digital integration time 2 s and bandwidth 1 nm over three accumulations).

Cooperativity of the DNA assemblies. Studies to monitor the cooperativity were carried using a quartz cuvette with a path length of 1 mm on a Jasco-810 spectropolarimeter equipped with a xenon lamp, a Peltier temperature control unit (at 5 °C) and a water recirculator. TA/Mg^{2+} buffer was employed in the samples, and used as a blank for all experiments.

Ultraviolet spectra. The DNA strand and MA were dissolved in TAE/Mg^{2+} buffer (150 μl) and annealed from 50 to 4 °C over 2 h. TAE/Mg^{2+} buffer (MA) was used as a blank. The ultraviolet spectra were measured on an Agilent Technologies CARY Series UV-Vis-NIR spectrophotometer at room temperature (230 to 350 nm range, 50 nm min^{-1} scan rate).

DLS spectra. DLS experiments were performed on a Brookhaven photon correlation spectrometer equipped with a BI9000 AT digital correlator. A Compass 315M-150 laser (Coherent Technologies) was used at 532 nm as an incident light source. A refrigerated recirculator was used to control the sample temperature. Autocorrelation functions were analysed using the CONTIN algorithm. Borosilicate glass sample vials were purchased from Canadawide Scientific. Samples were prepared in TA/Mg^{2+} buffer, and the reagents were filtered through 0.45-μm-nylon syringe filters prior to incubation.

Job's plot procedure. A series of solutions that contained T_{50} (1 equiv.) and MA (50 molecules = 1 equiv.) were prepared such that the total sum of the poly(T) and MA concentrations remained constant. The mole fraction of MA was varied from 0.1 to 1.0 and the solutions analysed by CD spectroscopy. The corrected ellipticity (mole fraction × ellipticity) at 278 nm was plotted against the molar fraction of MA. The intersection of two linear lines was used to deduce the product stoichiometry.

Crystallization. DNA oligonucleotides were purchased from IDT. Crystals were grown using the hanging drop vapour diffusion method by combining 4 μl of the oligonucleotides (0.5 μg $μl^{-1}$) solution that contained 20 mM MA with 5 μl of growing buffer (pH 7.0) that containing 0.002 M magnesium chloride hexahydrate, 0.005 M MOPS, 0.2 M ammonium sulfate and 0.00005 M spermine. Ammonium sulfate (2 M) was used as the reservoir buffer. Cubic-shaped crystals with dimensions as large as 150 μm × 150 μm × 150 μm were obtained after incubation for 4–7 days at 20 °C. Crystals were then transferred with cryoloops into a drop of cryoprotectant and allowed to incubate for 1 min before being frozen by liquid nitrogen. Cryoprotectant was prepared with one drop of 4 μl of 0.2× TAE/Mg^{2+} buffer with 5 μl of growing buffer (pH 7.0) that contained 0.002 M magnesium chloride hexahydrate, 0.005 M MOPS, 0.2 M ammonium sulfate and 0.00005 M spermine (and 3% 2-methyl-2,4-pentanediol) and was incubated against 600 μl of 2 M ammonium sulfate overnight (the volume shrunk to 1/10).

Data collection, processing and structure solution. X-ray diffraction data were collected on a Rigaku RU-H2R rotating anode X-ray machine at 1.54 Å. All the data were indexed, refined, integrated and scaled using HKL2000. The crystal belonged to the space group *I*23. The structure was solved using the molecular replacement method. A model of six nucleotides as a DNA single strand (triplex-forming strand, TCTCTC, then the sequence was mutated to TTTTTT in COOT by the 'Calculate—Model/Fit/Refine—Simple Mutate') cut from a triplex model (1d3x)[49] was used as the initial search model. The Phaser-MR program in the PHENIX package was used for molecular replacement. The resulting $F_o - F_c$ difference map was used to determine the positions of the MA molecules. MA molecules were added manually one by one using COOT, followed by rounds of refinements using phenix.refine after the addition of each MA molecule. Finally, the poly(T)–MA triplet was treated as one rigid body during refinement. In later rounds, real-space, atom occupancies, B-factor and *XYZ* coordinates were refined. In further refinements, magnesium atoms and a sulfate ion contained in the crystallization buffer were modelled into large difference peaks in the difference map. Final statistics are given in Supplementary Table 2. The atomic coordinates and structure factors have been deposited in the Protein Data Bank with accession codes 6WK7. All of the figures were generated with COOT and PyMOL. The DNA structure parameters (twist and rise) were analysed with 3DNA (Web 3DNA 2.0 for the analysis, visualization and modelling of 3D nucleic acid structures, http://web.x3dna.org/).

Assembly of individual DNA tiles. DNA single strands were mixed in their designated ratios in TAE/Mg^{2+} buffer to give a final 1 μM DNA solution. The DNA solutions were then incubated at 95 °C for 5 min, 65 °C for 30 min, 50 °C for 30 min, 37 °C for 30 min, 22 °C for 30 min and then 4 °C for 60 min. PAGE was conducted in the presence of 10 mM MA, if necessary. The running buffer was the TAE/Mg^{2+} buffer. Gels were run on a FB-VE10-1 electrophoresis unit (FisherBiotech) at 4 °C (300 V, constant voltage) for 2 or 3 h. After electrophoresis, the gels were stained with Stains-All dye (Sigma) and scanned.

Assembly of DNA arrays. DNA single strands were mixed in their designated ratios in TAE/Mg^{2+} buffer (supplemented with 10 mM MA) to give a final 1 μM DNA solution. The DNA solutions were then incubated at 95 °C for 5 min, 65 °C for 30 min, 50 °C for 30 min, 37 °C for 30 min, 22 °C for 30 min and then 4 °C for 60 min.

AFM. DNA solution (20 μl) was deposited onto a freshly cleaved mica surface and incubated for 5 min. Without further treatment, AFM images were captured by a MultiMode 8 (Bruker) using ScanAsyst-fluid mode with ScanAsyst-fluid+ probes (Bruker) in the DNA sample buffer. The tip–surface interaction was automatically adjusted to optimize the scan set point.

Synthesis of DNA constructs for mechanochemical experiments. The DNA constructs that contain a DNA hairpin were sandwiched between two long dsDNA handles (2,028 and 2,690 bp) (Supplementary Fig. 10). The-biotin labelled 2,028-bp dsDNA handle was prepared by PCR amplification using a pBR322 template (New England Biolab (NEB)) and a 5′-biotinylated primer 5′-GCA TTA GGA AGC AGC CCA GT AGTA GG-3′ (IDT). The PCR product was subsequently digested with XbaI restriction enzyme (NEB). The 2,690-bp dsDNA handle was prepared from pEGFP plasmid by sequential digestion using SacI (NEB) and EagI (NEB) restriction enzymes. This handle was subsequently labelled at the 3′-end (SacI) by digoxigenin using 18 μM DIG–dUTP (Roche) and terminal transferase (Fermentas).

To synthesize the 20 T-T DNA construct (Supplementary Fig. 10a), oligo 1 was annealed with oligo 2 and oligo 3. The final DNA construct was synthesized using T4 DNA ligase (NEB) through sequential two-piece ligations (1:1 molar ratio), starting with the ligation between the 2,028 dsDNA handle and the hairpin-containing fragment, followed by ligation to the 2,690 dsDNA handle via the respective cohesive ends.

To synthesize the 20 A-T DNA construct (Supplementary Fig. 10b), oligo 4, which contained a part of the hairpin stem (12 nucleotides, underlined), was annealed with oligo 2 at 97 °C for 5 min and slowly cooled to room temperature for 6 h. This fragment was ligated with the 2,028-bp DNA handle by T4 DNA ligase (NEB) and gel purified using a kit (Midsci). On the other side of the DNA construct, oligo 6, which contained another part of the hairpin stem, was annealed with oligo 3. This fragment was ligated with the 2,690-bp handle and gel purified. The final DNA construct was synthesized using T4 DNA ligase (NEB) through three-piece ligation of the 2,028 and 2,690-bp DNA handles and oligo 5, which contained a 4-nucleotide loop with underlined regions that represented the complementary regions of the hairpin stem.

To synthesize the RCA constructs used for mechanical chemical sensing (Fig. 6), we first circularized the 5′-phosphorylated linear template (5′-GTCGTGAT-A_{44}-CAATCCTG) with a splint (5′-GCA TTA GGA AGC AGC CCA GTA GTA GGA TCA CGA CCA GGA TTG) using T4 DNA ligase at 16 °C for 16 h. The splint was removed by a splint remover that contained sequence complementary to the splint. The obtained circular DNA templates were then annealed with the biotinylated primer (/5′-Bio/-GCA TTA GGA AGC AGC CCA GTA GTA GGA TCA CGA CCA GGA TTG). RCAs were carried out using Phi 29 enzyme (NEB) at 37 °C for 10 min to obtain linear single-stranded DNA. The resulting linear DNA strands were labelled with digoxigenin using DIG–dUTP (Roche) and terminal transferase (Thermo Fisher) at 37 °C for 3 h.

Single-molecule mechanical unfolding experiments. The experiment was conducted on a homebuilt laser tweezers instrument for the single-molecule experiment[50]. To perform the mechanochemical experiment, 2 μl of a diluted DNA construct (~1 ng μl^{-1}) was incubated with 1 μl of a 0.1% solution of streptavidin-coated polystyrene beads (diameter, 1.87 μm; Spherotech) for about 30 min at room temperature (25 °C), which immobilized the DNA construct on the bead surface through streptavidin–biotin complex formation. The incubated sample was further diluted to 1 ml in TAE/Mg^{2+} buffer and injected into the top channel of a three-channel microfluidic chamber. Polystyrene beads (2 μl, diameter 2.10 μm) coated anti-digoxigenin antibodies were also dispersed into the same buffer (1 ml) and injected into the bottom channel of the three-channel microfluidic chamber. Two separate laser beams derived from the same diode-pumped solid-state laser (1,064 nm, 5 W; IPG Photonics) were used to trap two different types of beads. The DNA construct was tethered between the two beads in the middle channel by escorting one of the trapped beads closer to another using a steerable mirror (Madcity Labs Inc.). In the ramping *F–X* mode, the steerable mirror that controls the streptavidin-coated bead was moved away from the antibody-coated bead with a loading speed of ~ 5.5 pN s^{-1}. The hairpin structure underwent an unfolding transition when the tension inside the tether was gradually increased. This transition was manifested with a sudden change in the end-to-end distance during the process. The single tether was confirmed by a single breakage event or a DNA overstretching plateau at 65 pN in the *F–X* curves. The *F–X* curve for each tether was recorded in a Labview 8 program (National Instruments Corp.), and data treatment was performed using Matlab (The MathWorks) and Igor (WaveMetrics) programs. The unfolding force was measured directly from the *F–X* curves, whereas ΔL due to the unfolding was calculated by the two data points that flanked a rupture event using an extensible worm-like chain model:

$$\frac{\Delta x}{\Delta L} = 1 - \frac{1}{2}\left(\frac{k_B T}{FP}\right)^{\frac{1}{2}} + \frac{F}{S} \quad (1)$$

where Δx is the change in extension between the data points of the stretching and relaxing curves at the same force (F), k_B is the Boltzmann constant, T is absolute temperature, P is the persistent length (50.8 ± 1.5 nm), F is the force and S is the elastic stretch modulus (1,243 ± 63 pN). When the molecule was relaxed with the same loading speed, the hairpin refolded, manifested by a sudden change in force or end-to-end distance in the *F–X* curve.

Single-molecule mechanochemical sensing experiments. Single-molecule mechanochemical sensing using the poly(T) RCA product was performed in a microfluidic chamber. The buffer only and buffer with target (MA) were flown in the top and bottom microfluidic channels, respectively. Poly(T) RCA products were tethered between a streptavidin-coated bead and an anti-digoxigenin-coated bead in a 10 mM Tris buffer (pH 7.4 supplemented with 100 mM KCl). After the two different beads were trapped separately by the two laser foci in the optical tweezers instrument (see previous section), the force ramping experiment was carried out in the buffer channel (top channel). The same molecule was then taken to the MA target channel (bottom channel). The binding of MA was detected by the sudden drop of the force signal in *F–X* traces.

Calculation of the expected ΔL. ΔL can be calculated using the equation:

$$\Delta L = L - \Delta x = NL_{nt} - \Delta x \quad (2)$$

where N is the number of nucleotides contained in the structure, L_{nt} is the contour length per nucleotide (~0.45 nm) and Δx is the end-to-end distance (~ 2 nm, the diameter of dsDNA). According to equation (2), the theoretical ΔL for a hairpin (52 nt = 24-bp stems and 4-nucleotide loops) unfolding was calculated as ~21.4 nm (52 nt × 0.45 nm/nt – 2 nm = 21.4 nm).

Reporting summary. Further information on research design is available in the Nature Research Reporting Summary linked to this article.

Data availability

Crystallography data (Fig. 3) are available from the Protein Data Bank (https://www.rcsb.org/) with access code 6WK7. The source data related to Figs. 4 and 5 are available upon request from the corresponding authors. All other data in the paper are provided as Source data.

References

49. Tarköy, M., Phipps, A. K., Schultze, P. & Feigon, J. Solution structure of an intramolecular DNA triplex linked by hexakis(ethylene glycol) units: d(AGAGAGAA-$(EG)_6$-TTCTCTCT-$(EG)_6$-TCTCTCTT). *Biochemistry* **37**, 5810–5819 (1998).
50. Mao, H. & Luchette, P. An integrated laser-tweezers instrument for microanalysis of individual protein aggregates. *Sens. Actuators B* **129**, 764–771 (2008).

Acknowledgements

This work was financial support by ONR (N00014-15-1-2707) and NSFC (21974111) to C.M., National Science Foundation (CBET-1904921) and National Institutes of Health (NIH 1R01CA236350) (in part) to H.M., the Natural Sciences and Engineering Research Council (NSERC) of Canada and the Canada Research Chairs Program to H.F.S. and F.J.R., and the Government of Canada for a Banting Fellowship to F.J.R.

Author contributions

H.F.S., H.M. and C.M supervised the project. Q.L. and S.W. conducted PAGE analyses. J.Z. and H.H. conducted crystallographic analysis. L.L. conducted AFM imaging. S.J. and S.M. conducted mechanical measurements. Q.L. and F.J.R. conducted CD, thermal denaturation and assembly mechanism experiments. All the authors contributed to the data analysis and the writing of the manuscript.

Competing interests

The authors declare no competing interests.

Additional information

Supplementary information is available for this paper at https://doi.org/10.1038/s41563-020-0728-2.

Correspondence and requests for materials should be addressed to H.F.S., H.M. or C.M.

Reprints and permissions information is available at www.nature.com/reprints.

nature research

Corresponding author(s): Chengde Mao

Last updated by author(s): May 26, 2020

Reporting Summary

Nature Research wishes to improve the reproducibility of the work that we publish. This form provides structure for consistency and transparency in reporting. For further information on Nature Research policies, see Authors & Referees and the Editorial Policy Checklist.

Statistics

For all statistical analyses, confirm that the following items are present in the figure legend, table legend, main text, or Methods section.

n/a	Confirmed
☐	☒ The exact sample size (*n*) for each experimental group/condition, given as a discrete number and unit of measurement
☐	☒ A statement on whether measurements were taken from distinct samples or whether the same sample was measured repeatedly
☒	☐ The statistical test(s) used AND whether they are one- or two-sided *Only common tests should be described solely by name; describe more complex techniques in the Methods section.*
☒	☐ A description of all covariates tested
☒	☐ A description of any assumptions or corrections, such as tests of normality and adjustment for multiple comparisons
☒	☐ A full description of the statistical parameters including central tendency (e.g. means) or other basic estimates (e.g. regression coefficient) AND variation (e.g. standard deviation) or associated estimates of uncertainty (e.g. confidence intervals)
☒	☐ For null hypothesis testing, the test statistic (e.g. *F*, *t*, *r*) with confidence intervals, effect sizes, degrees of freedom and *P* value noted *Give P values as exact values whenever suitable.*
☒	☐ For Bayesian analysis, information on the choice of priors and Markov chain Monte Carlo settings
☒	☐ For hierarchical and complex designs, identification of the appropriate level for tests and full reporting of outcomes
☒	☐ Estimates of effect sizes (e.g. Cohen's *d*, Pearson's *r*), indicating how they were calculated

Our web collection on statistics for biologists contains articles on many of the points above.

Software and code

Policy information about availability of computer code

Data collection	None
Data analysis	Labview 8; Matlab 7.1; Igor 6.2; HKL2000_712-Linux; WinCoot 0.7.2.1; Phaser 2.8.0 in the PHENIX package; phenix.refine (PHENIX 1.12-2829); Pymol 1.6.0.0; Web 3DNA 2.0.

For manuscripts utilizing custom algorithms or software that are central to the research but not yet described in published literature, software must be made available to editors/reviewers. We strongly encourage code deposition in a community repository (e.g. GitHub). See the Nature Research guidelines for submitting code & software for further information.

Data

Policy information about availability of data

All manuscripts must include a data availability statement. This statement should provide the following information, where applicable:

- Accession codes, unique identifiers, or web links for publicly available datasets
- A list of figures that have associated raw data
- A description of any restrictions on data availability

protein data band (pdb) access id: 6WK7

Field-specific reporting

Please select the one below that is the best fit for your research. If you are not sure, read the appropriate sections before making your selection.

☒ Life sciences ☐ Behavioural & social sciences ☐ Ecological, evolutionary & environmental sciences

Life sciences study design

All studies must disclose on these points even when the disclosure is negative.

Sample size	sample sizes are 89 and 86 in the two figures used in Fig. 4d, respectively.
Data exclusions	no
Replication	yes
Randomization	No.
Blinding	No.

Reporting for specific materials, systems and methods

We require information from authors about some types of materials, experimental systems and methods used in many studies. Here, indicate whether each material, system or method listed is relevant to your study. If you are not sure if a list item applies to your research, read the appropriate section before selecting a response.

Materials & experimental systems

n/a	Involved in the study
☒	☐ Antibodies
☒	☐ Eukaryotic cell lines
☒	☐ Palaeontology
☒	☐ Animals and other organisms
☒	☐ Human research participants
☒	☐ Clinical data

Methods

n/a	Involved in the study
☒	☐ ChIP-seq
☒	☐ Flow cytometry
☒	☐ MRI-based neuroimaging